The sequestration efficiency of the biological pump

Tim DeVries,[1] Francois Primeau,[2] and Curtis Deutsch[1]

Received 9 April 2012; revised 29 May 2012; accepted 31 May 2012; published 3 July 2012.

[1] The conversion of dissolved nutrients and carbon to organic matter by phytoplankton in the surface ocean, and its downward transport by sinking particles, produces a "biological pump" that reduces the concentration of atmospheric CO_2. Global rates of organic matter export are a poor indicator of biological carbon storage however, because organic matter gets distributed across water masses with diverse pathways and timescales of return to the surface. Here we show that organic matter export and carbon storage can be related through a sequestration efficiency, which measures how long regenerated nutrients and carbon will be stored in the interior ocean before being returned to the surface. For the first time, we derive global maps of the sequestration efficiency of the biological pump at different residence time horizons. These maps reveal how regional patterns of organic matter export contribute to the biological pump, and how the biological pump responds to changes in biological productivity driven by climate change.
Citation: DeVries, T., F. Primeau, and C. Deutsch (2012), The sequestration efficiency of the biological pump, *Geophys. Res. Lett.*, *39*, L13601, doi:10.1029/2012GL051963.

1. Introduction

[2] The ocean's carbon reservoir exceeds chemical equilibrium with the atmosphere because the deep ocean is a repository for CO_2 and nutrients released during the decomposition of organic matter falling from the surface ocean. Diagnostic calculations [e.g., *Ito and Follows*, 2005] reveal that while deep ocean nutrients are partly derived from regenerated organic matter, a comparable fraction is transported from surface waters where limitations on plankton growth prevent complete nutrient consumption. These "preformed" nutrients do not contribute to biological carbon storage, implying that the biological pump is not operating at maximum efficiency. Changes in the efficiency of the biological pump, as measured by the fraction of nutrients in the regenerated pool, therefore have the potential to alter ocean carbon storage and atmospheric CO_2 over time [*Sigman and Boyle*, 2000; *Ito and Follows*, 2005; *Marinov et al.*, 2008a, 2008b].

[3] The fact that no quantitative relationship has been demonstrated between the rate of organic matter export and the efficiency of the biological pump represents a significant shortcoming in our understanding of the global carbon cycle, and our ability to link changes in ocean productivity and atmospheric CO_2. Indeed, it is often noted that global rates of organic matter export can increase even while the efficiency of the biological pump decreases [*Matsumoto*, 2007; *Marinov et al.*, 2008a; *Kwon et al.*, 2011]. This ambiguity stems from the fact that organic matter settling out of the euphotic zone may be stored for as little as months or as long as a millennium before returning to the surface, depending on where the export occurs and the depth at which it is regenerated.

[4] Here we show that the strength of the biological pump can be related directly to the rate of organic matter export, Φ_{ex}, by considering the *sequestration efficiency* $\mathcal{E}(\tau|\mathbf{r})$ of regenerated nutrients. $\mathcal{E}(\tau|\mathbf{r})$ is equal to the proportion of nutrients regenerated from organic matter exported out of the euphotic zone below point $\mathbf{r}$ that remain sequestered below the surface for a period τ or longer (see methods and Figure S1 in the auxiliary material).[1] The inventory of regenerated nutrients can be expressed as a convolution of $\mathcal{E}$ with Φ_{ex}, allowing the biological pump efficiency E_{bio} to be expressed as

$$E_{bio}(t) = \frac{1}{I_{tot}(t)} \int_a da \int_0^\infty d\tau \mathcal{E}(\tau|\mathbf{r}) \Phi_{ex}(\mathbf{r}, t-\tau), \qquad (1)$$

where I_{tot} is the ocean's nutrient inventory, a is the ocean surface area and t is calendar time. E_{bio} varies between 0 (no biological pump) and 1 (perfectly efficient biological pump). Equation (1) is strictly valid for the case of steady circulation but can be generalized to the case of non-stationary flow. The advantage of expressing E_{bio}, a globally integrated metric, using equation (1) is that it provides a direct connection to the time-dependent export production on regional scales.

2. Temporal and Spatial Dependence of the Sequestration Efficiency

[5] We estimated $\mathcal{E}$ using a data-constrained ocean circulation and biogeochemistry model (see Appendix A). By construction, $\mathcal{E} = 1$ everywhere at $\tau = 0$. As τ increases, upwelling and eddy-diffusion return nutrients to the surface where they are removed from the regenerated pool (see Appendix B), so that $\mathcal{E} \to 0$ as $\tau \to \infty$. At $\tau = 1$ year, some regions have lost as much as 50% of the initial pool of regenerated nutrients (Figure 1). Such low sequestration efficiencies are associated with regions of persistent upwelling or rapid vertical exchange, for example, along the northern flank of the Gulf Stream, in the Peru and Benguela upwelling systems, and in some parts of the Southern Ocean. By $\tau = 10$ years the highest sequestration efficiencies are

[1]Department of Atmospheric and Oceanic Sciences, University California, Los Angeles, California, USA.
[2]Earth System Science Department, University of California, Irvine, California, USA.

Corresponding author: T. DeVries, Department of Atmospheric and Oceanic Sciences, University California, Los Angeles, CA 90095, USA. (tdevries@atmos.ucla.edu)

0094-8276/12/2012GL051963

[1]Auxiliary materials are available in the HTML. doi:10.1029/2012GL051963.

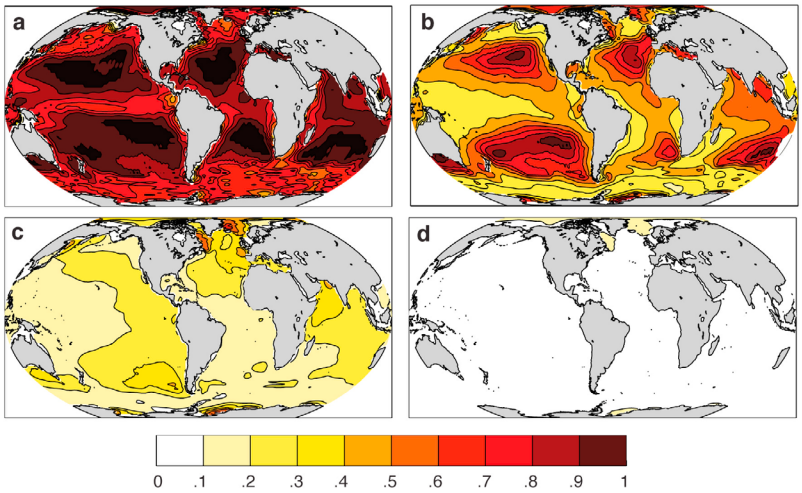

Figure 1. The sequestration efficiency of exported organic matter, $\mathcal{E}(\tau|\mathbf{r})$, is shown for (a) τ = 1 year, (b) τ = 10 years, (c) τ = 100 years, and (d) τ = 1000 years. Here and in Figure 2 all fields have been smoothed with a 200 km Gaussian averaging filter before plotting, to suppress grid-scale noise and to focus on large-scale patterns.

found in subtropical gyre regions where remineralized nutrients are downwelled by Ekman convergence. At τ = 100 years, the areas which feed the deep ocean circulation increasingly stand out, with $\mathcal{E}$ exceeding 50% in areas where North Atlantic Deep Water and Antarctic Bottom Water are produced. Sequestration efficiencies over most of the rest of the ocean have dropped to around 10–30% after 100 years. By τ = 1000 years, only small amounts of regenerated nutrients remain, mainly originating from regions of deep convection in the Labrador Sea and Greenland-Iceland-Norwegian seas in the North Atlantic, and from the Weddell Sea in the Southern Ocean. A small proportion of the regenerated nutrients derived from organic matter exported from these regions is transported into the deep limb of the global overturning circulation, where it is sequestered for more than a thousand years.

3. Mean Sequestration Time and Regional Biological Pump Efficiencies

[6] It is widely thought that variations in biological pump efficiency are important drivers of glacial-interglacial variations in atmospheric CO_2 [*Broecker*, 1982; *Sigenthaler and Wenk*, 1984; *Sarmiento and Toggweiler*, 1984; *Knox and McElroy*, 1984; *Sigman and Boyle*, 2000; *Sigman et al.*, 2010]. For persistent quasi-stationary patterns of organic matter export associated with the ~100,000 year periods of glacial-interglacial cycles, the export rate $\Phi_{ex}(\mathbf{r}, t)$ can be approximated by its time average, $\overline{\Phi}_{ex}(\mathbf{r})$, so that equation (1) simplifies to

$$\overline{E}_{bio} \approx \frac{1}{I_{tot}} \int_a R(\mathbf{r}) \overline{\Phi}_{ex}(\mathbf{r}) da, \qquad (2)$$

where $\mathcal{R}(\mathbf{r}) = \int_o^\infty \mathcal{E}(\tau|\mathbf{r}) d\tau$ is the mean sequestration time of regenerated nutrients originating from organic matter sinking out of the euphotic zone below **r**. Figure 2 shows $\mathcal{R}(\mathbf{r})$ estimated using our data-constrained model, revealing a structure similar to that shown in the longer timescales of Figure 1. Maximum mean sequestration times of 400+ years are found in the high-latitude deep-water formation regions of the North Atlantic and Southern Ocean. Mean sequestration times generally decrease away from these regions. In the North Atlantic, there is a gradual transition from regions of high sequestration efficiency in the polar regions to regions of low sequestration efficiency in the tropics (except near the Gulf Stream region where the transition is abrupt) (Figure 2b). By contrast, the transition between regions of high- and low-sequestration times in the Southern Ocean is well-defined and abrupt. Waters along the Antarctic coast in the Weddell Sea (Figure 2c), and to a lesser extent the Ross Sea, have very high

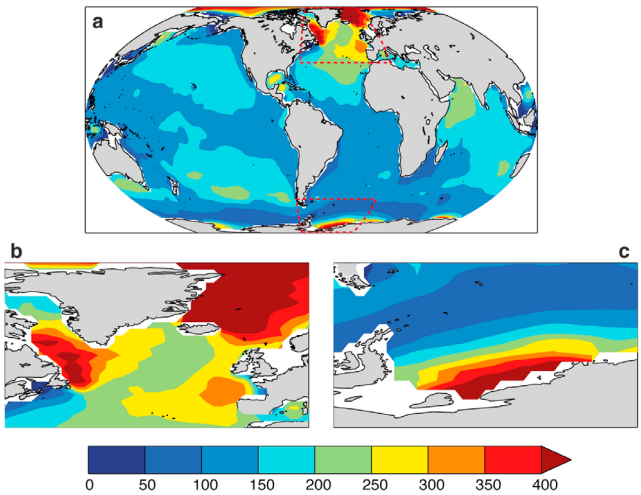

Figure 2. On long timescales, the sequestration efficiency of the biological pump can be characterized by the mean sequestration time of regenerated organic matter. (a) Spatial variability in this sequestration time results from the global pattern of ocean circulation, with high sequestration times in areas where deep and bottom waters form, and low sequestration times in areas of persistent upwelling. Subplots (marked by dashed red lines in Figure 2a) highlight the divides between regions of high and low sequestration efficiency in (b) the North Atlantic and (c) the Weddell Sea region of the Southern Ocean. Timescale is in years.

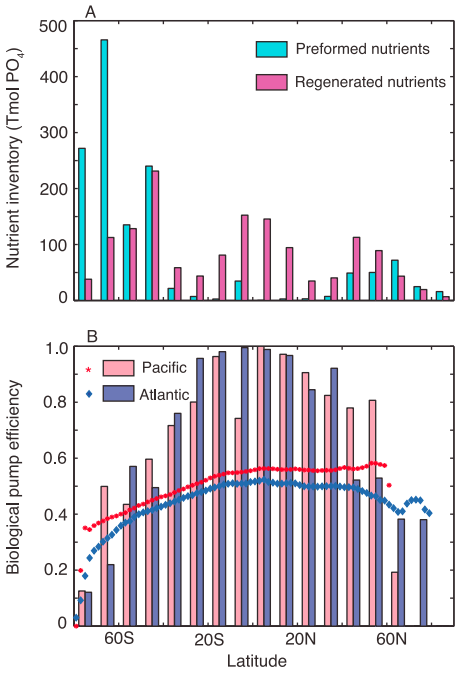

Figure 3. (a) The contribution by latitude of ventilation (preformed nutrients, which reduce the efficiency of the biological pump) and organic matter export (regenerated nutrients, which enhance the efficiency of the biological pump) to the total nutrient inventory of the contemporary ocean. Bar heights represent amount of nutrients exported from the surface ocean, as calculated using equations (B1) and (B2) by integrating over 10° latitude bins. (b) The efficiency of the biological pump in the Atlantic and Pacific Oceans. Bars are efficiencies calculated from the total amount of regenerated and preformed nutrients originating from each 10° latitude bin as defined in Figure 3a, and symbols are efficiencies calculated from the modeled distribution of preformed and regenerated nutrients in the interior ocean.

sequestration times, while elsewhere Southern Ocean waters have some of the lowest sequestration times of any open ocean waters (<100 years). Short sequestration times in the Southern Ocean are associated with strong Ekman upwelling that returns deep waters to the surface [*Toggweiler and Russell*, 2008], while the long sequestration times are associated with deep convection along the Antarctic margin [*Marinov et al.*, 2006]. Deep convection does not occur in the Pacific and Indian Oceans, so mean sequestration times in these ocean basins are relatively uniform at ~100–200 years, with longer sequestration times associated with areas of sub-tropical mode water formation and the poorly-ventilated shadow zone in the Arabian Sea.

[7] In the contemporary ocean, the distribution of mean sequestration times (Figure 2) and organic matter export rates is such that regenerated nutrients are supplied mainly by organic matter exported from the sub-polar and tropical regions (Figure 3a) (see Appendix B). However, these regions only export enough organic matter to account for about half of the total nutrient inventory, such that $E_{bio} = 0.5$ in the data-constrained model. The remaining 50% of nutrients are preformed nutrients supplied by waters ventilated primarily in the Southern Ocean, and to a lesser extent the North Atlantic (Figure 3a).

[8] The efficiency of the biological pump for a particular oceanic region can be expressed as the ratio of the total amount of regenerated nutrients supplied to the interior ocean by organic matter export within that region, to the sum of the regenerated and preformed nutrients delivered to the interior ocean from that region. This calculation reveals that the biological pump is inefficient at high latitudes, with efficiencies of 0.1–0.4 in polar regions, and that efficiencies increase to near 1 in the tropics (Figure 3b). The global efficiency of the biological pump (0.5) reflects a balance between nutrients supplied from high-efficiency regions (mainly the tropics) and nutrients supplied from low-efficiency regions (primarily the Southern Ocean). Subpolar regions also supply significant amounts of nutrients (Figure 3a), with biological pump efficiencies near the global mean (Figure 3b).

[9] The view of regional biological pump efficiency derived here is different from that derived using interior distributions of regenerated nutrients [e.g., *Williams and Follows*, 2011]. Because nutrients are transported and mixed within the ocean, interior nutrient distributions reflect non-local biological processes, and therefore do not reflect the efficiency of the biological pump acting in surface waters in that region. This can be seen by comparing the efficiencies calculated here with those calculated from the ratio of regenerated to total nutrients in the model (Figure 3b). In regions where a single locally-ventilated water mass dominates, such as near the Antarctic margin or in the North Atlantic, the two approaches give approximately the same efficiency. But in regions where water masses mix, such as the equatorial regions, the regional efficiencies inferred from the two approaches diverge (Figure 3b). Efficiencies calculated using interior nutrient distributions tend to reflect the basin-scale average efficiency (around 0.4 in the Atlantic and 0.6 in the Pacific), while efficiencies calculated using organic matter export rates and sequestration efficiencies reflect local surface biological efficiency.

[10] At the global scale the two approaches should in principle yield the same biological pump efficiency, since all regenerated nutrients in the interior ocean are derived from organic matter exported from the surface ocean. In practice, interior distributions of regenerated nutrients are often calculated from the observed apparent oxygen utilization (AOU) using constant stoichiometries [e.g., *Ito and Follows*, 2005]. Thus the difference between the globally-integrated biological pump efficiency estimated here ($E_{bio} = 0.5$) and a previous estimate ($E_{bio} = 0.36$) based on AOU [*Ito and Follows*, 2005] is due to errors in the estimation of regenerated nutrients by the two methods, including uncertain stoichiometry of organic matter in the case of estimates based on AOU, and errors in the circulation and remineralization rates in the case of the model-based estimate (see discussion in the auxiliary material).

4. Biological Pump Response to Long-Term Changes in Organic Matter Export

[11] On long time horizons the strength of the biological pump, as measured by the inventory of regenerated nutrients [*Ito and Follows*, 2005; *Marinov et al.*, 2008a, 2008b], is governed by the mean sequestration time of regenerated nutrients, and the mean rate of organic matter export (see

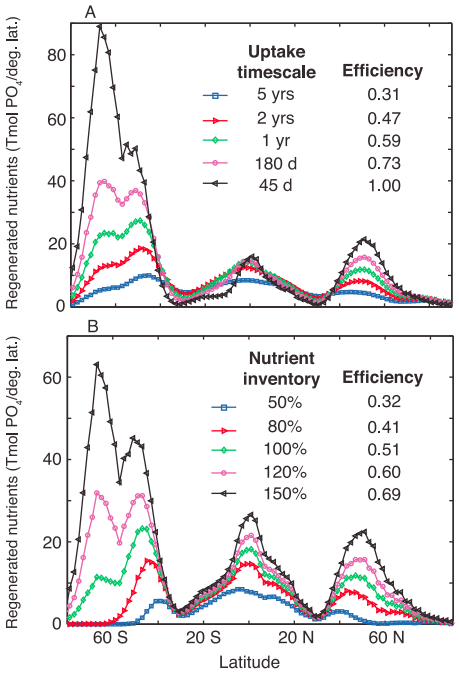

Figure 4. The response of the biological pump, as measured by the amount of regenerated nutrients supplied by organic matter exported from the surface ocean (equation (B2)), under two idealized scenarios: (a) the biological uptake timescale is varied between 5 years and 45 days (complete nutrient depletion), and (b) the total oceanic nutrient inventory is varied from 50% to 150% of the modern inventory. The globally-integrated biological pump efficiency (equation (2)) is printed in each plot. Nutrient inventories have been averaged at neighboring latitudes in order to reduce grid-scale noise.

equation (2)). Over glacial-interglacial cycles, variability in organic matter export rates may be driven by variability in aeolian iron deposition [*Martin*, 1990; *Wolff et al.*, 2006] or by variability in the ocean's total nutrient inventory [*Ganeshram et al.*, 1995; *Falkowski*, 1997; *Ganeshram et al.*, 2000, 2002]. Here we explore how the strength of the biological pump responds to changes in organic matter export rates in a series of idealized simulations (see Appendix C). We maintain a constant circulation and therefore constant sequestration efficiency, although this is also likely to change over time due to changes in surface winds and buoyancy forcing.

[12] An idealized simulation of the effects of iron deposition is obtained by depleting surface nutrients to varying levels (Figure 4a). For slow nutrient uptake rates (τ_b = 5 years) associated with strong iron limitation, the biological pump is inefficient and the delivery of regenerated nutrients is relatively constant by latitude. As nutrient uptake rates increase, more regenerated nutrients are delivered by organic matter exported from the Southern Ocean, the tropics, and the sub-Arctic regions. For $\tau_b \lesssim 45$ days, surface nutrients are completely consumed and the biological pump reaches maximum efficiency. In this case nutrients are consumed directly where they are upwelled, showing that the majority of ocean waters upwell in the Southern Ocean, the tropics, and in the sub-Arctic (mainly the North Pacific) [*DeVries and Primeau*, 2011]. The biological pump response to variations in total nutrient inventory is somewhat different (Figure 4b). As in the nutrient depletion scenario (Figure 4a), the response is most pronounced in the Southern Ocean. However, the response is also significant in the tropics and the sub-Arctic, suggesting that these regions may be important drivers of variability in the biological pump over glacial-interglacial cycles if the cycles are accompanied by large changes in the ocean's nutrient inventory.

[13] Overall these idealized experiments support the view that the Southern Ocean plays a central role in modulating the biological pump efficiency [*Sarmiento and Toggweiler*, 1984; *Sigenthaler and Wenk*, 1984; *Knox and McElroy*, 1984; *Sigman and Boyle*, 2000; *Sigman et al.*, 2010]. However, the Southern Ocean control of the biological pump is significantly weaker in the case that the total nutrient content varies, as opposed to the more commonly considered case of nutrient depletion [*Sarmiento and Orr*, 1991; *Marinov et al.*, 2006].

5. Conclusion

[14] A traditional paradigm holds that the efficiency of the biological pump is controlled by the preformed nutrient content of the ocean [*Sigman and Boyle*, 2000; *Ito and Follows*, 2005; *Marinov et al.*, 2008a, 2008b]. This view is useful for quantifying how bulk changes in oceanic nutrient concentrations affect atmospheric CO_2 concentrations [*Ito and Follows*, 2005; *Marinov et al.*, 2008a, 2008b], but cannot be used to describe how the biological pump responds to regional changes in the rate of organic matter export. Here we proposed an alternate view based on the idea that the inventory of regenerated nutrients in the ocean can be expressed as the convolution of the organic matter export rate with a sequestration efficiency function $\mathcal{E}$. This sequestration efficiency is spatially variable, reaching maximum values in areas of deep convection where the densest water masses are formed. For the contemporary ocean, we find that biological pump efficiencies are highest in the tropics and lowest in the polar regions, with intermediate efficiencies in the sub-polar regions. Assuming modern-day sequestration efficiency patterns continue to hold, the response of the biological pump to changes in organic matter export is likely to be dominated by the Southern Ocean, with secondary contributions from the tropical and sub-Arctic regions.

Appendix A: Data-Constrained Circulation and Biogeochemistry Model

[15] The model resolution is 2 degrees in the horizontal with 24 vertical levels. The circulation is steady-state and is meant to represent a climatological mean ocean circulation [*DeVries and Primeau*, 2011]. The model has been fit to climatological temperature, salinity, and natural radiocarbon distributions using an adjoint method as described elsewhere [*DeVries and Primeau*, 2011]. We have extended this work to include a simple biogeochemistry model for the production and remineralization of particulate organic phosphate, and adding the 2009 World Ocean Atlas gridded phosphate concentrations [*Garcia et al.*, 2010] as an additional observational constraint. Export production is modeled by restoring to observed phosphate in the top two model layers

wherever modeled PO_4 is greater than observed PO_4 with a timescale τ_b = 30 days,

$$\Phi_{ex}(\mathbf{r}) = \frac{1}{\tau_b} \times \max\left(\mathrm{PO}_4(\mathbf{r}) - \mathrm{PO}_4^{obs}(\mathbf{r}), 0\right) \quad \text{(A1)}$$

Organic matter exported out of the euphotic zone is assumed to remineralize in the interior ocean following a power-law relationship [*Martin et al.*, 1987],

$$J(\mathbf{r}, z) = \frac{\partial}{\partial z}\left(\Phi_{ex}(\mathbf{r}) \times \left(\frac{z}{z_c}\right)^{-b}\right), \quad \text{(A2)}$$

where the compensation depth z_c = 73 m, which corresponds to the top two layers of the model. The attenuation coefficient b is determined as part of the solution to the inverse model, and b = 0.82 at the optimal solution. The globally integrated rate of export production in the model is 9.4 × 10^{12} mol P yr^{-1}. Comparison between model-simulated and observed PO_4 is given in the auxiliary material (Figure S2).

Appendix B: Preformed and Regenerated Nutrients

[16] For purposes of this study all nutrients in the production zone above the compensation depth z_c (hereafter, "surface nutrients") are considered preformed nutrients. At steady state, the inventory I_{pref} of preformed nutrients in the ocean can be expressed as the convolution of the surface nutrient concentration and the boundary propagator Green function $\mathcal{G}(\mathbf{r})$,

$$\mathrm{I}_{pref} = \int_a \mathcal{G}(\mathbf{r}) c(\mathbf{r}) da + \int_a \int_{z=0}^{z=z_c} c(\mathbf{r}) dz da, \quad \text{(B1)}$$

where c is a generic nutrient (phosphate in our model). $\mathcal{G}(\mathbf{r})$ represents the volume of the interior ocean (below the euphotic zone) ventilated per unit surface area at point $\mathbf{r}$, and has units of meters [*Primeau*, 2005]. The total amount of nutrients in the ocean is the sum of the preformed and regenerated components, $\mathrm{I}_{tot} = \mathrm{I}_{pref} + \mathrm{I}_{reg}$, where the regenerated nutrient inventory at steady state is given by the numerator in equation (2)

$$\mathrm{I}_{reg} = \int_a \mathcal{R}(\mathbf{r}) \overline{\Phi}_{ex}(\mathbf{r}) da. \quad \text{(B2)}$$

Changing the limits of integration in (B1) and (B2) from the whole ocean to an arbitrary region of the surface ocean yields the total amount of preformed or regenerated nutrients delivered to the interior ocean from that particular region, as in Figure 3.

Appendix C: Production Scenarios

[17] Nutrient depletion experiments (Figure 4a) were performed by setting $\mathrm{PO}_4^{obs}(\mathbf{r}) = 0$ in equation (A1) and varying the biological uptake timescale τ_b from 5 years to 45 days. The total amount of nutrients in the ocean was kept constant at modern levels for these experiments. To simulate the effect of adding or removing nutrients from the ocean (Figure 4b) we retained the production parameterization of equation (A1) but varied the total phosphate inventory from 50% to 150% of the modern inventory.

[18] **Acknowledgments.** Constructive comments from two anonymous reviewers helped improve the paper. Funding for this research was provided by NSF grant OCE-1131548 and NSF grant OCE-1131768.

[19] The Editor thanks two anonymous reviewers for assisting in the evaluation of this paper.

References

Broecker, W. (1982), Glacial to interglacial changes in ocean chemistry, *Prog. Oceanogr.*, *11*, 151–197.

DeVries, T., and F. Primeau (2011), Dynamically- and observationally-constrained estimates of water-mass distributions and ages in the global ocean, *J. Phys. Oceangr.*, *41*(12), 2378–2398.

Falkowski, P. G. (1997), Evolution of the nitrogen cycle and its influence on the biological sequestration of CO_2 in the ocean, *Nature*, *387*, 272–276.

Ganeshram, R. S., T. F. Pedersen, S. E. Calvert, and J. W. Murray (1995), Large changes in oceanic nutrient inventories from glacial to interglacial periods, *Nature*, *376*, 755–758.

Ganeshram, R. S., T. F. Pedersen, S. E. Calvert, G. W. McNeill, and M. R. Fontugne (2000), Glacial-interglacial variability in denitrification in the world's oceans: Causes and consequences, *Paleoceanography*, *15*, 361–376.

Ganeshram, R. S., T. F. Pedersen, S. E. Calvert, and R. Francois (2002), Reduced nitrogen fixation in the glacial ocean inferred from changes in marine nitrogen and phosphorus inventories, *Nature*, *415*, 156–159.

Garcia, H. E., R. A. Locarnini, T. P. Boyer, J. I. Antonov, M. M. Zweng, O. K. Baranova, and D. R. Johnson (2010), *World Ocean Atlas 2009*, vol. 4, *Nutrients (Phosphate, Nitrate, Silicate)*, edited by S. Levitus, 398 pp., NOAA, Silver Spring, Md.

Ito, T., and M. Follows (2005), Preformed phosphate, soft tissue pump and atmospheric CO_2, *J. Mar. Res.*, *63*, 813–839.

Knox, F., and M. B. McElroy (1984), Changes in atmospheric CO_2: Influence of the marine biota at high latitude, *J. Geophys. Res.*, *89*(D3), 4629–4637.

Kwon, E. Y., J. L. Sarmiento, J. R. Toggweiler, and T. DeVries (2011), The control of atmospheric pCO_2 by ocean ventilation change: The effect of the oceanic storage of biogenic carbon, *Global Biogeochem. Cycles*, *25*, GB3026, doi:10.1029/2011GB004059.

Marinov, I., A. Gnanadesikan, J. R. Toggweiler, and J. L. Sarmiento (2006), The Southern Ocean biogeochemical divide, *Nature*, *441*, 964–967.

Marinov, I., A. Gnanadesikan, J. L. Sarmiento, J. R. Toggweiler, M. Follows, and B. K. Mignone (2008a), Impact of oceanic circulation on biological carbon storage in the ocean and atmospheric pCO_2, *Global Biogeochem. Cycles*, *22*, GB3007, doi:10.1029/2007GB002958.

Marinov, I., M. Follows, A. Gnanadesikan, J. L. Sarmiento, and R. D. Slater (2008b), How does ocean biology affect atmospheric pCO_2? Theory and models, *J. Geophys. Res.*, *113*, C07032, doi:10.1029/2007JC004598.

Martin, J. (1990), Glacial-interglacial CO_2 change: The iron hypothesis, *Paleoceangraphy*, *5*, 1–13.

Martin, J., G. Knauer, D. Karl, and W. Broenkow (1987), VERTEX: Carbon cycling in the northeast Pacific, *Deep Sea Res., Part A*, *34*, 267–285.

Matsumoto, K. (2007), Biology-mediated temperature control on atmospheric pCO_2 and ocean biogeochemistry, *Geophys. Res. Lett.*, *34*, L20605, doi:10.1029/2007GL031301.

Primeau, F. (2005), Characterizing transport between the surface mixed layer and the ocean interior with a forward and adjoint global ocean transport model, *J. Phys. Oceangr.*, *35*(4), 545–564, doi:10.1175/JPO2699.1.

Sarmiento, J. L., and J. C. Orr (1991), Three-dimensional ocean model simulations of the impact of Southern Ocean nutrient depletion on atmospheric CO_2 and ocean chemistry, *Limnol. Oceanogr.*, *36*, 1928–1950.

Sarmiento, J. L., and J. R. Toggweiler (1984), A new model for the role of the oceans in determining atmospheric pCO_2, *Nature*, *308*, 621–624.

Sigenthaler, U., and T. Wenk (1984), Rapid atmospheric CO_2 variations and ocean circulation, *Nature*, *308*, 624–626.

Sigman, D. M., and E. A. Boyle (2000), Glacial/interglacial variations in atmospheric carbon dioxide, *Nature*, *308*, 859–869.

Sigman, D. M., M. P. Hain, and G. H. Haug (2010), The polar ocean and glacial cycles in atmospheric CO_2 concentration, *Nature*, *446*, 47–55, doi:10.1038/nature09149.

Toggweiler, J. R., and J. Russell (2008), Ocean circulation in a warming climate, *Nature*, *451*, 286–288.

Williams, R. G., and M. J. Follows (2011), *Ocean Dynamics and the Carbon Cycle: Principles and Mechanisms*, 404 pp., Cambridge Univ. Press, Cambridge, U. K.

Wolff, E. W., et al. (2006), Southern Ocean sea-ice extent, productivity and iron flux over the past eight glacial cycles, *Nature*, *440*, 491–496.